



Global observations  
of fire NO<sub>x</sub> emissions

A. K. Mebust and  
R. C. Cohen

This discussion paper is/has been under review for the journal Atmospheric Chemistry and Physics (ACP). Please refer to the corresponding final paper in ACP if available.

# Space-based observations of fire NO<sub>x</sub> emission coefficients: a global biome-scale comparison

A. K. Mebust<sup>1</sup> and R. C. Cohen<sup>1,2</sup>

<sup>1</sup>Department of Chemistry, University of California at Berkeley, Berkeley, California, USA

<sup>2</sup>Department of Earth and Planetary Science, University of California at Berkeley, Berkeley, California, USA

Received: 22 July 2013 – Accepted: 15 August 2013 – Published: 22 August 2013

Correspondence to: R. C. Cohen (rccohen@berkeley.edu)

Published by Copernicus Publications on behalf of the European Geosciences Union.

Title Page

Abstract

Introduction

Conclusions

References

Tables

Figures



Back

Close

Full Screen / Esc

Printer-friendly Version

Interactive Discussion



## Abstract

Biomass burning represents both a significant and highly variable source of  $\text{NO}_x$  to the atmosphere. This variability stems from both the episodic nature of fires, and from fire conditions such as the modified combustion efficiency of the fire, the nitrogen content of the fuel and possibly other factors that have not been identified or evaluated by comparison with observations. Satellite instruments offer an opportunity to observe emissions from wildfires, providing a large suite of measurements which allow us to study mean behavior and variability on the regional scale in a statistically rigorous manner. Here we use space-based measurements of fire radiative power from the Moderate Resolution Imaging Spectroradiometer in combination with  $\text{NO}_2$  tropospheric column densities from the Ozone Monitoring Instrument to measure mean emission coefficients (ECs in  $\text{g NO MJ}^{-1}$ ) from fires for global biomes, and across a wide range of smaller-scale ecoregions, defined as spatially-distinct clusters of fires with similar fuel type. Mean ECs for all biomes fall between  $0.250\text{--}0.362 \text{ g NO MJ}^{-1}$ , a range that is smaller than found in previous studies of biome-scale emission factors. The majority of ecoregion ECs fall within or near this range, implying that under most conditions, mean fire emissions per unit energy are similar between different regions regardless of fuel type or spatial variability. In contrast to these similarities, we find that about 24% of individual ecoregion ECs deviate significantly ( $p < 0.05$ ) from the mean EC for the associated biome, and a similar number of ecoregion ECs falls outside this range, implying that there are some regions where fuel type-specific global emission parameterizations fail to capture local fire  $\text{NO}_x$  emissions.

## 1 Introduction

Biomass burning emissions induce a variety of effects to climate and air quality. They impact the global radiative budget directly by absorbing or reflecting incoming radiation, e.g.  $\text{CO}_2$  and aerosols, and/or indirectly by influencing the chemistry of climate forcers,

## Global observations of fire $\text{NO}_x$ emissions

A. K. Mebust and  
R. C. Cohen

Title Page

Abstract

Introduction

Conclusions

References

Tables

Figures



Back

Close

Full Screen / Esc

Printer-friendly Version

Interactive Discussion



**Global observations  
of fire NO<sub>x</sub> emissions**A. K. Mebust and  
R. C. Cohen

Title Page

Abstract

Introduction

Conclusions

References

Tables

Figures

◀

▶

◀

▶

Back

Close

Full Screen / Esc

Printer-friendly Version

Interactive Discussion



e.g. nitrogen oxides (NO<sub>x</sub> = NO + NO<sub>2</sub>) and CO acting as ozone (O<sub>3</sub>) precursors (Bowman et al., 2009; Fiore et al., 2012; Jaffe and Wigder, 2012). NO<sub>x</sub>, O<sub>3</sub> and aerosols also have negative health impacts, especially at high concentrations. Understanding, quantifying and mitigating these effects requires an understanding of both the magnitude of the emissions, and their variability across a range of spatial and temporal scales.

Current models of fire emissions rely on a biomass-burned approach: to estimate the mass of a compound emitted, an empirically measured emission factor (EF) is multiplied by an estimate of the total biomass burned, often calculated as the product of other factors (e.g. burn area, fuel loading, combustion completeness) that are simpler to measure or estimate (Andreae and Merlet, 2001; Wiedinmyer et al., 2006; van der Werf et al., 2010). This strategy has weaknesses, as the uncertainty in biomass burned for a particular fire is high, and even aggregate estimates at lower spatial and temporal resolution can have significant biases (van der Werf et al., 2010; Granier et al., 2011). Additionally, measured EFs vary greatly between individual fires due to differences in fire conditions, e.g. fuel type, structure, moisture, etc. (Andreae and Merlet, 2001; Korontzi et al., 2003; van Leeuwen and van der Werf, 2011; van Leeuwen et al., 2013). In this work, we focus on emissions of NO<sub>x</sub>, which are produced in wildfires as the result of oxidative combustion of nitrogen (N) contained in the biomass (Andreae and Merlet, 2001). Measured NO<sub>x</sub> EFs for fires are generally considered to be positively correlated with modified combustion efficiency (MCE) and fuel N content (e.g. Lacaux et al., 1996; Battye and Battye, 2002). A high MCE indicates a greater contribution of higher-temperature flaming combustion which is thought to oxidize the N more effectively, while high fuel N provides a larger source of N to ultimately be oxidized to NO<sub>x</sub> (Andreae and Merlet, 2001). However, observational evidence confirming these effects is limited. Observed correlations between NO<sub>x</sub> EFs and MCE are typically poor (e.g. Battye and Battye, 2002; Yokelson et al., 2011), and fuel nitrogen content is rarely quantified. Models of fire NO<sub>x</sub> emissions typically use EFs for a few (3–7) fuel types, based on averages of EFs measured for fires of each particular fuel type (e.g. Andreae and Merlet, 2001; Hoelzemann et al., 2004; van der Werf et al., 2010; Ak-

**Global observations  
of fire NO<sub>x</sub> emissions**A. K. Mebust and  
R. C. Cohen[Title Page](#)[Abstract](#)[Introduction](#)[Conclusions](#)[References](#)[Tables](#)[Figures](#)[⏪](#)[⏩](#)[◀](#)[▶](#)[Back](#)[Close](#)[Full Screen / Esc](#)[Printer-friendly Version](#)[Interactive Discussion](#)

agi et al., 2011). The number of fires from which each EF is derived ranges from a handful (3–5) to tens or perhaps even hundreds, depending on the fuel type and the emitted species in question. However, even when EFs are derived from large numbers of fires, these observations come from only a few targeted measurement campaigns that sample many fires with fuels comprised of a relatively small range of plant species and over a short temporal span (e.g. Akagi et al., 2011). This raises the question of whether the observations are representative of variations in emissions that would be observed under a more spatially and temporally comprehensive sampling strategy that incorporates spatially distinct fire regimes with the same fuel type and covers seasonal and interannual variations in rainfall, wind speed and other climatic conditions.

Several satellite instruments measure fire-related properties, providing data that span the globe, have full annual coverage, and sample many fires in each region, allowing for statistical evaluation of variance in emissions and reducing the potential for bias due to an unrepresentative sample. Deriving an EF from satellite observations, however, is challenging due to the difficulty in estimating biomass burned in the fire and connecting that information to instantaneous measurements of atmospheric composition. Instead, methods for estimating the mass of a pollutant emitted per unit radiative energy released from the fire – a value we define as the emission coefficient (EC) to distinguish it from the EF – have been developed (Ichoku and Kaufman, 2005; Jordan et al., 2008; Vermote et al., 2009; Mebust et al., 2011; Mebust and Cohen, 2013). The idea for an EC was born out of laboratory work that established a linear relationship between the amount of energy released by a fire and the total biomass burned, suggesting that (a) an energy-based parameterization is a logical alternative to a mass-based one, and (b) measured ECs should be proportional to EFs (Wooster, 2002; Wooster et al., 2005; Freeborn et al., 2008). ECs provide a straightforward way to estimate EFs from satellite observations because measurements of fire radiative power (FRP) are made daily with near-global coverage from the two Moderate Resolution Imaging Spectroradiometer (MODIS) instruments, allowing for simultaneous estimation of en-

ergy and pollutant emissions for any species measured from space near the MODIS overpass times.

In two previous papers, we developed a method to combine global observations of FRP from MODIS with  $\text{NO}_2$  tropospheric column density measurements from the Ozone Monitoring Instrument (OMI) to calculate ECs for  $\text{NO}_x$  and assessed the method as applied to fires in California and Nevada, and also examined seasonal variability in ECs in African savannas (Mebust et al., 2011; Mebust and Cohen, 2013). Here we adapt this method to provide a global picture of variations in  $\text{NO}_x$  emissions. We calculate ECs for several global biomes and for different ecoregions within these biomes, and describe how these ECs compare to each other and to EFs reported in previous studies.

## 2 Data

This analysis incorporates information from OMI, MODIS, a climate classification system, and the Climate Forecast System Reanalysis (CFSR) and Version 2 Reforecast (CFSv2). We use global observations from years 2005–2011.

### 2.1 OMI

OMI is a nadir-viewing spectrometer onboard the polar-orbiting EOS-Aura satellite, with an equatorial overpass time of  $\sim 1:45$  p.m. (local time). OMI measures the solar irradiance and backscatter radiance from earth at UV and visible wavelengths (270–500 nm with 0.5 nm resolution) to derive column densities for several trace gases. We use tropospheric vertical  $\text{NO}_2$  column densities obtained from the OMI  $\text{NO}_2$  standard product (OMNO2, Level 2, Version 2.1, Collection 3). The retrieval process for these columns is described in detail elsewhere (Bucsela et al., 2013); briefly, slant  $\text{NO}_2$  columns are derived using differential optical absorption spectroscopy (DOAS), separated into stratospheric and tropospheric components, and converted to vertical column densities using

Title Page

Abstract

Introduction

Conclusions

References

Tables

Figures

◀

▶

◀

▶

Back

Close

Full Screen / Esc

Printer-friendly Version

Interactive Discussion



Global observations  
of fire NO<sub>x</sub> emissionsA. K. Mebust and  
R. C. Cohen

Title Page

Abstract

Introduction

Conclusions

References

Tables

Figures

◀

▶

◀

▶

Back

Close

Full Screen / Esc

Printer-friendly Version

Interactive Discussion



an air mass factor, which is derived from several parameters including terrain reflectivity and height and an estimated NO<sub>2</sub> vertical profile. The spatial footprint is 13 × 24 km<sup>2</sup> at nadir. We use data from the inner 40 (of 60) across-track pixels, omitting the low spatial resolution observations at the edge of the swath. We also limit observations to those with a cloud fraction of less than 20 %, as pixels with a high cloud fraction have reduced sensitivity to NO<sub>2</sub> below the clouds (Boersma et al., 2002), and we reject all pixels affected by the row anomaly.

It is plausible that the a priori NO<sub>2</sub> vertical profile shapes used in the retrieval process might lead to a bias in measured NO<sub>2</sub> columns over smoke plumes. The OMNO2 standard product v2.1 uses GMI CTM monthly mean modeled NO<sub>2</sub> vertical profile shapes at 2° × 2.5° (Bucsela et al., 2013). Previous work has identified a negative bias over persistent features smaller than this model resolution that results from the low spatial resolution of the estimated NO<sub>2</sub> profile. Specifically, Russell et al. (2011) developed a regional OMI NO<sub>2</sub> retrieval and found that urban NO<sub>2</sub> columns increased by 8 %, and this increase was primarily attributed to using WRF-Chem profiles at 4 km × 4 km resolution as opposed to the lower resolution profiles in the NASA standard product v1.0. This is consistent with the observation by Boersma et al. (2011) that when near-surface NO<sub>2</sub> gradients were less strong, it resulted in a decrease in measured NO<sub>2</sub> for a different retrieval of OMI, because a larger fraction of NO<sub>2</sub> was distributed relatively higher in the atmosphere where the OMI instrument sensitivity is higher. Given that fires are episodic, heavy-emitting point sources in regions that are typically remote with few NO<sub>x</sub> emission sources, the assumed NO<sub>2</sub> vertical profile will have very little NO<sub>2</sub> distributed in the lowest layer as compared to the “true” NO<sub>2</sub> vertical profile over most fires. This difference will be much more pronounced than in an urban area where the assumed profile, while diluted over a large spatial scale, still represents some of the vertical gradient over a NO<sub>x</sub> source, and thus we expect a much larger bias. The impact of high aerosol loading may also have an effect, as one study considered the effects of mixed and/or layered aerosol and NO<sub>2</sub> on the NO<sub>2</sub> retrieval and found that effects are theoretically small when NO<sub>2</sub> and aerosol are collocated but much larger of

the aerosol is above or below the plume (Leitao et al., 2010). However, the importance of this effect to our work is uncertain, as it is expected that fresh smoke plumes will generally contain well-mixed NO<sub>2</sub> and aerosol. Regardless, there is a theoretical basis for a low bias in OMI NO<sub>2</sub> measurements over smoke plumes.

In Mebust et al. (2011) we found that EFs derived from measurements of MODIS FRP and OMI NO<sub>2</sub> were lower than reference EFs by a factor of approximately 2–5 (depending on the reference EF). The source of that discrepancy is not understood, although it potentially stems in part from the aforementioned low bias in OMI NO<sub>2</sub> over fires. However, we do not believe it varies in a statistically representative ensemble of fires, and thus relative differences in ECs are believed to be reliable.

## 2.2 MODIS

MODIS instruments operate on NASA's Aqua and Terra satellites. MODIS measures spectral radiance in 36 bands which cover visible and IR wavelengths. We use the Thermal Anomalies product (MYD14, Level 2, Collection 5) and the Land Cover product (MCD12Q1, Level 3, Collection 5.1). We only include fires detected by the Aqua MODIS instrument during daytime, as this allows near-coincident measurement of fires and NO<sub>2</sub> column densities. Fires are detected using the 4 μm and 11 μm bands; pixels with elevated radiance in these bands as compared to surrounding pixels are labeled as containing fire. The spatial resolution of the bands is 1 × 1 km<sup>2</sup>, but the algorithm is sensitive enough to detect fires as small as 100 m<sup>2</sup>. An estimate of pixel FRP is derived from the 4 μm brightness temperature. Further details on the fire detection and FRP estimation algorithms are discussed elsewhere (Kaufman et al., 1998; Justice et al., 2002; Giglio et al., 2003)

It has been suggested that there exists a low bias in MODIS FRP resulting from reduced sensitivity to radiance under conditions where fires are too small to be detected, obscured by clouds or canopy cover, or burning below ground (e.g. Wooster et al., 2003; Boschetti and Roy, 2009; Vermote et al., 2009; Freeborn et al., 2011). In this analysis we minimize most of these biases because we use only detected fires

Title Page

Abstract

Introduction

Conclusions

References

Tables

Figures

◀

▶

◀

▶

Back

Close

Full Screen / Esc

Printer-friendly Version

Interactive Discussion



**Global observations  
of fire NO<sub>x</sub> emissions**A. K. Mebust and  
R. C. Cohen

Title Page

Abstract

Introduction

Conclusions

References

Tables

Figures

◀

▶

◀

▶

Back

Close

Full Screen / Esc

Printer-friendly Version

Interactive Discussion



and compare with NO<sub>2</sub> columns directly over the source. In most of these cases, the percentage of undetected FRP due to undetected or cloud-obscured actively burning locations is likely small. Nevertheless, our analysis may be sensitive to canopy effects or underground burning, particularly because we consider relative differences in ECs between different biomes where this effect may vary in magnitude. A low bias in FRP in particular biomes would elevate reported EC values in those biomes.

Land cover classifications are assigned to 500 × 500 m<sup>2</sup> pixels using the International Geosphere-Biosphere Programme (IGBP) classification (Friedl et al., 2010). We assume that land cover in 2011 is the same as in 2010 because at the time of this analysis, the land cover product was only available for years 2005–2010. The IGBP classification scheme provides 17 different categorizations of land type; we assign many of these categories to biome categories as shown in Table 1, but occasionally use the direct IGBP classifications.

### 2.3 Köppen-Geiger climate classification

Common EF schemes distinguish between tropical, temperate, and boreal forests; to identify these distinct forest types we use the Köppen-Geiger global climate classification system at 0.5° × 0.5° resolution (Kottek et al., 2006). This dataset classifies climate as one of five main climate types (“equatorial,” “arid,” “warm temperate,” “snow,” “polar”), with additional sub-classifications related to precipitation and temperature. We classify forests as “tropical” if they are found in “equatorial” climates, “temperate” if they are found in “arid” or “warm temperate” climates, and “boreal” if they are found in “snow” or “polar” climates. We also use sub-classifications of the “equatorial” regime (“fully humid,” “monsoonal” and “winter-dry”) to separately examine differences in tropical evergreen vs. tropical dry deforestation.

## 2.4 CFSR, CFSv2

The CFSR is a global reanalysis and forecast for years from 1979 through 2010; CFSR was extended starting in 2011 using CFSv2 and continues as an operational real-time product (Saha et al., 2010, 2013). Wind fields used in this work are from the 850 hPa vertical level (corresponding to approximately 1.5 km altitude) and are available at  $0.5^\circ \times 0.5^\circ$  resolution hourly. The reanalysis is performed with 6 h time steps and this is coupled with forecasts to provide output for every hour.

## 3 Methodology

We build on the methodology described in Mebust et al. (2011), which was adapted from Ichoku and Kaufman (2005). All fire pixels detected by the Aqua MODIS instrument daytime overpasses during 2005–2011 are assigned a land type using the MODIS land cover product for the appropriate year (or 2010 for fire pixels detected in 2011) and matched with OMI pixels coincident in time and space. OMI pixels that contain fire pixels with FRP above 250 MW are aggregated using a sorting algorithm such that adjacent OMI pixels are analyzed as a single fire “event”. We note that Mebust et al. (2011) included OMI pixels containing less than 250 MW of FRP. Globally, we observed that there are many regions where fires occur more densely than in California and Nevada. Here, we chose the 250 MW criterion because we determined through testing that it was the minimum possible cutoff at which most pixels in these fire-dense regions did not aggregate into extremely large groups; we also calculated that under standard conditions of wind speed and predicted emission rates, the change in column density of  $\text{NO}_2$  over an individual fire with FRP equal to 250 MW would generally be below the detection limit of OMI. To further ensure removal of data that cannot be attributed to an individual fire, we did not analyze any fire events that were greater in size than 3 OMI pixels in the along-track dimension or 2 OMI pixels in the across-track direction.

Title Page

Abstract

Introduction

Conclusions

References

Tables

Figures

◀

▶

◀

▶

Back

Close

Full Screen / Esc

Printer-friendly Version

Interactive Discussion



Global observations  
of fire NO<sub>x</sub> emissionsA. K. Mebust and  
R. C. Cohen

Title Page

Abstract

Introduction

Conclusions

References

Tables

Figures

◀

▶

◀

▶

Back

Close

Full Screen / Esc

Printer-friendly Version

Interactive Discussion



The total mass of NO<sub>2</sub> emitted by each fire was calculated using the total area of OMI pixels in the event and the column density of NO<sub>2</sub> over the fire after subtracting a background column density, calculated using fire-free OMI observations in the same location covering a period of 60 days before and 60 days after the fire. Events for which there were less than 10 valid background observations were considered to have a poorly characterized background column and were not analyzed further. Tests in Mebust and Cohen (2013) established that deriving the background from a smaller range of observations (e.g. 30 days before and 30 days after) reduced the observational sample size but did not otherwise affect the results. The time over which the observed NO<sub>2</sub> was emitted, the “clear time”, was then calculated using the wind speed and direction near the fire, the OMI pixel edges, and the center of the fire, calculated as the mean of fire pixel locations weighted by pixel FRP. Dividing the mass of NO<sub>2</sub> emitted by the clear time yields the mass emission rate (MER), or rate at which the fire is emitting NO<sub>2</sub> as observed by the satellite. This is not, however, the direct NO<sub>2</sub> EC from the fire, since the NO<sub>2</sub> observed by satellite is at photostationary state. We assume that at photostationary state, 75 % of NO<sub>x</sub> is present as NO<sub>2</sub> to obtain the EC for NO<sub>x</sub>. This assumption is consistent with previous in situ measurements which typically find that NO<sub>2</sub> constitutes 50–100 % of NO<sub>x</sub>. Since we are concerned with relative comparisons of EFs, it is important to establish that this fraction will not vary significantly as a result of background ozone concentration. We estimate that the impact from this effect is small because our ECs scale by (NO + NO<sub>2</sub>):NO<sub>2</sub> rather than the direct ratio NO:NO<sub>2</sub>, and calculate that factor-of-two differences in background ozone will result in <20 % change to (NO + NO<sub>2</sub>):NO<sub>2</sub>. In Mebust and Cohen (2013) we presented evidence that seasonal variations in NO<sub>x</sub> ECs in African savannas were not primarily driven by changes in background ozone.

Satellite observations of fire plumes inevitably contain a mix of fresh (immediately over the source) and aged (downwind) emissions. Although the OMI spatial resolution is relatively high, NO<sub>x</sub> loss is fast enough (lifetime on the scale of hours) that significant loss of NO<sub>x</sub> can occur by the time the plume reaches the edge of the OMI pixel. We

correct for this effect using a 1-D model and 2 h lifetime assumption as described in Mebust et al. (2011). All data subsequently presented in this paper has been adjusted using this model and assumed lifetime.

To ensure the data is representative of emissions from fires, we remove points with high background column density ( $3.5 \times 10^{15}$  molecules  $\text{cm}^{-2}$ ), or either long ( $> 3$  h) or short ( $< 15$  min) clear times. Observations with a high background tend to yield higher uncertainty in calculated mass of  $\text{NO}_2$  emitted by the fire; long clear times increase the likelihood that the fire violates the assumption that the fire properties have not changed significantly over the time of observation; and short clear times can result in an anomalously high (or negative) MER as the clear time appears in the denominator of the MER, amplifying uncertainty in the difference between the observed  $\text{NO}_2$  column density over the fire and the background  $\text{NO}_2$  column density. Approximately 30 % of observations are removed by these filters.

We present results for all fires of a particular fuel type across the globe (i.e. a “biome-scale” EC) and for spatially distinct clusters of fires of similar fuel types (i.e. an “ecoregion-scale” EC). Fire biomes are identified using primary land cover type (for all fires) and climate classifications (for forests). To be classified as a particular biome type, 75 % of FRP from a fire must come from fire pixels identified as that biome type. We use a spatial clustering method to further classify fires into ecoregions; fires of an individual fuel type (e.g forests) that occur within 250 km (100 km for grasses) of each other are grouped and each group is considered an ecoregion for the purpose of this analysis. ECs for both biomes and ecoregions are derived via linear regression with nonparametric bootstrap resampling (5000 resamples). The intercept is not forced through zero to account for any possible small bias in emission estimates from low-energy fires. Typically we require at least 100 observations to consider an EC adequately constrained. We also remove extreme high-weight points by removing all points that affect the fit by 100 % or more. There are only two ecoregions (and no biomes) that contain points that fall into this category; one ecoregion contained one such point and

## Global observations of fire $\text{NO}_x$ emissions

A. K. Mebust and  
R. C. Cohen

[Title Page](#)[Abstract](#)[Introduction](#)[Conclusions](#)[References](#)[Tables](#)[Figures](#)[◀](#)[▶](#)[◀](#)[▶](#)[Back](#)[Close](#)[Full Screen / Esc](#)[Printer-friendly Version](#)[Interactive Discussion](#)



number of observations. As this number increases, the parameters are less likely to be anomalously high or low, and so the standard error decreases.

We demonstrate the natural variability (with contributions from individual measurement uncertainty) by calculating ECs directly (dividing MER by FRP) for fires of all fuel types with high FRP ( $> 5000 \text{ MJ s}^{-1}$ ); we note that the standard deviation is the square root of the variance. The distribution, with both arithmetic and geometric mean and standard deviation, of the directly-calculated ECs is shown in Fig. 2. The arithmetic standard deviation of ECs is 72 % of the arithmetic mean. However, the distribution is not normal, limiting the value of arithmetic statistics. A log-normal distribution and geometric statistics offer a better description of the observations. The geometric mean for a log-normal distribution is equal to the median; the geometric standard deviation is a multiplicative factor rather than an additive one. In this case, a geometric standard deviation of  $\sim 2$  indicates that approximately 68 % of observations are contained between one-half and twice the geometric mean. Another way to highlight the natural variability of ECs between individual fires is to consider the  $R^2$  value, which is also the fraction of explained variance. An  $R^2$  of  $\sim 0.3$  (as observed in the case of most of our biome-scale ECs) indicates that about 70 % of the variance is unexplained by a linear relationship between FRP and MER.

Despite the large variance, however, most of our ECs have a relatively low standard error (15 % or lower). This is because of the large number of observations that factor into each EC. Uncertainty in the best fit (i.e. the EC) is given by the standard error, which is the estimated standard deviation of the best fit parameter (i.e. the slope) as the experiment is repeated with the same number of observations. In our case, we use nonparametric bootstrap resampling to calculate the EC. One advantage of the bootstrap is that it provides a direct estimate of this distribution of variability in the best fit parameter via the distribution of bootstrap resamples. Therefore we can estimate the standard error in our ECs by calculating the standard deviation of the bootstrap resamples. We use this method to provide the standard error of all ECs presented in

Global observations  
of fire  $\text{NO}_x$  emissionsA. K. Mebust and  
R. C. Cohen

Title Page

Abstract

Introduction

Conclusions

References

Tables

Figures

◀

▶

◀

▶

Back

Close

Full Screen / Esc

Printer-friendly Version

Interactive Discussion



this work. The bootstrap resamples are generally normally distributed, so we provide arithmetic standard deviations as our estimate of the standard error.

## 4.2 Spatial variability within biomes

5 Within each biome there are several spatially distinct ecoregions. We calculate 45 ECs for 42 separate ecoregions; forests are not separated by climate classification for the purposes of determining ecoregions, but for the three forest ecoregions with sufficient sampling of multiple forest biomes, we include multiple ECs. Maps of ecoregions and corresponding ECs are shown in Figs. 3–6; ECs,  $R^2$  and  $N$  for each ecoregion are available in tables in the Supplement. We also calculate  $p$  values for statistical testing  
10 directly using bootstrap distributions of the difference between each ecoregion EC and the mean EC for that biome. We find that most (34 out of 45, or  $\sim 75\%$ ) ecoregion ECs are not statistically significantly different than the mean biome EC at the 0.05 level. However, there are ecoregions with statically significantly different ECs in all biomes. We include the  $p$  value in the Supplement Tables for these cases. When differences  
15 between ecoregion and mean biome ECs are statistically significant, they tend to be large, with most differences ranging from 50% to more than a factor of 2.

### 4.2.1 Forests

Figure 3 shows a map of all forest ecoregions containing more than 100 separate observations and ECs for those ecoregions. Fires from clusters with fewer than 100  
20 observations are shown in black. ECs are calculated separately for each biome category (e.g. tropical vs. temperate forest) and biomes are indicated by marker shape. The range of mean biome ECs for all biomes is indicated in grey. We find that one of six tropical forest ecoregion ECs is significantly different from the mean tropical forest EC (Region B); similarly, one of six temperate forest ecoregion ECs is significantly different  
25 from the mean temperate forest EC (Region G). One of two boreal forest ecoregion

## Global observations of fire NO<sub>x</sub> emissions

A. K. Mebust and  
R. C. Cohen

Title Page

Abstract

Introduction

Conclusions

References

Tables

Figures



Back

Close

Full Screen / Esc

Printer-friendly Version

Interactive Discussion



ECs is different from the mean boreal forest EC (Region K). Correlation coefficients ( $R^2$ ) for each ecoregion range between 0.1 and 0.5 (see Supplement).

#### 4.2.2 Grasses

Results for grass fire ecoregions are found in Fig. 4. These ecoregion ECs are the most variable of all the biomes; six of the seventeen ecoregions have ECs that are significantly different from the mean grassland EC (Regions L, P, R, X, Y, and Z). In these ecoregions, ECs range from as large as 0.95 to as small as 0.187 gNO MJ<sup>-1</sup>. However, ECs in the remaining ecoregions are all within 30% of the mean grassland EC. Correlation coefficients ( $R^2$ ) for each ecoregion range from 0.1 to 0.7; seven of the seventeen ecoregions have  $R^2$  greater than 0.4. Three of those have ECs that differ significantly from the mean (Regions X, Y and Z).

#### 4.2.3 Shrubs

The shrubland biome is not considered in most global treatments of fire NO<sub>x</sub> emissions, likely because there are few measurements of shrub EFs and shrub fires generally do not make up a large portion of the global biomass consumed by fire. These fires are (presumably) partitioned into other biome categories. Our mean biome EC for shrubs falls within the range of other mean biome ECs, suggesting that treating shrub fires as grass or forest fires would not cause a large bias in global total fire emissions. Results from our shrub ecoregion analysis are presented in Fig. 5. The range of variation is smaller than in other biomes, although one of five ecoregions is statistically significantly different from the mean shrub EC (Region DD). Correlation coefficients for these ecoregions are generally much higher than for ecoregions in other biomes, ranging from 0.3 to 0.7 with four of five regions having  $R^2 \sim 0.4$  or above. This may be due to better consistency in emission conditions as a result of the smaller size of the shrub regions vs. grass or forest regions and/or of the greater number of highly energetic fires

### Global observations of fire NO<sub>x</sub> emissions

A. K. Mebust and  
R. C. Cohen

Title Page

Abstract

Introduction

Conclusions

References

Tables

Figures

◀

▶

◀

▶

Back

Close

Full Screen / Esc

Printer-friendly Version

Interactive Discussion



as a percent of observations (> 10 % of observations have FRP above 2000 MJ s<sup>-1</sup> for shrub fires, as opposed to less than 10 % for grass and forest fires).

#### 4.2.4 Agriculture

Results for agricultural fires are presented in Fig. 6. Fire emissions of NO<sub>x</sub> from this biome are perhaps the hardest to characterize, because these controlled fires are usually small. This is reflected in the relatively larger uncertainties (see Fig. 6b) and also in much lower correlation coefficients;  $R^2$  is below 0.15 for all but one of the 9 crop regions shown below. Only one of the nine ecoregion ECs is statistically significantly different from the mean agricultural EC (Region NN); however, that may partly be due to the higher uncertainties in ECs for this crop type. Using a harvested crop area dataset (Monfreda et al., 2008), we identify the main crop type for most regions to be wheat, except Region HH (sorghum) and Regions KK and LL (soybeans). There is no obvious relationship between crop type and EC.

## 5 Discussion

### 5.1 Biome- and ecoregion-scale similarities and differences

Broadly, the ECs presented here suggest that mean fire behavior is similar regardless of biome or ecoregion. We find that 75 % of ecoregion ECs are not significantly different from the corresponding biome-scale EC. These ECs fall within 32 % of the mean biome EC for all biomes except agriculture, and for individual biomes the range can be as low as a few percent. Differences in the agricultural biome are larger partly because of larger uncertainties in the derived ECs. As previously noted, biome-scale ECs themselves cover a relatively narrow range (the lowest value is ~ 70 % of the highest value). We find that almost half of the ecoregion-scale ECs (21 out of 45) fall directly into this range, and 9 more overlap the range within the standard error of the EC. However,

## Global observations of fire NO<sub>x</sub> emissions

A. K. Mebust and  
R. C. Cohen

Title Page

Abstract

Introduction

Conclusions

References

Tables

Figures

◀

▶

◀

▶

Back

Close

Full Screen / Esc

Printer-friendly Version

Interactive Discussion



**Global observations  
of fire NO<sub>x</sub> emissions**A. K. Mebust and  
R. C. Cohen

Title Page

Abstract

Introduction

Conclusions

References

Tables

Figures

◀

▶

◀

▶

Back

Close

Full Screen / Esc

Printer-friendly Version

Interactive Discussion



there are several ecoregion-scale ECs that do not overlap this range within standard error or even twice the standard error. These ECs are generally substantially different (i.e. by 50 % or more) from the biome scale ECs. These differences suggest that emissions differ more with location than with fuel type, challenging the traditional model of emissions as fuel type-specific.

Ecoregions observed to deviate from mean ECs contain a moderate number of observations rather than a small number, suggesting that the differences are robust. The large differences in these ECs as compared to the mean biome EC will result in significant biases in emission estimates for these specific regions. The most notable of these is for boreal forest in Asia (Region K). Most conventional estimates of boreal forest NO<sub>x</sub> EFs are derived from measurements of fires in North America; however, we find that ECs in boreal forest in Asia are fully twice those in North America (Region J). This is particularly important because emissions from boreal forest fires lay an especially important role in global atmospheric composition and chemistry (Jacob et al., 2010; Simpson et al., 2011).

We do not fully understand causes of the observed ecoregion-scale differences. It is possible that differences in fuel *N* content and/or fire MCE are responsible, but evaluating these factors on the scale of an ecoregion requires an in-depth understanding of local fire behavior as well as observations of these factors that currently do not exist on the spatial or temporal scale of this analysis. Rather than speculating on specific causes here, we instead hope that identification of clear differences in different ecoregions guides future efforts to reveal and assess processes that govern fire emissions.

## 5.2 Comparison to previous work

We compare both to our previous work quantifying fire emissions from space, and to global biome EFs from conventional fire emission schemes.

## 5.2.1 California and Nevada revisited

In Mebust et al. (2011) we applied the same basic methodology with minor differences to fires over California and Nevada (126–113°W, 31–44°N) and found that our calculated MER was correlated with FRP with  $R^2$  ranging from 0.3 to 0.8, that relative differences in emissions between fuel types previously obtained by in situ measurements were reproduced by our analysis, and that the absolute values of the ECs and EFs we measured were several times smaller than previously obtained EF and EC measurements. In this work we update our analysis to incorporate a more recent version of the OMI NO<sub>2</sub> retrieval (Standard Product v2.1 vs. v1.0), a different wind dataset (CFSR winds at 850 hPa and 0.5° × 0.5° resolution vs. NARR winds at 900 hPa and 32 km resolution), additional years of observations (2009–2011), removal of OMI pixels containing less than 250 MW of total FRP from further analysis, and adjustments to how observations were selected for removal with respect to e.g. background, clear time, etc. Here we include a comparison to those previous results.

Figure 7 shows MER vs. FRP for (a) all fires, (b) forest fires, (c) shrub fires and (d) grass fires in the California/Nevada region indicated above. In most cases, the  $R^2$  for each category is slightly higher than observed in Mebust et al. (2011), possibly due to improvements in methodology, improvements to the NO<sub>2</sub> retrieval in the Standard Product v2.1 vs. v1.0, and/or a reduction in the number of points scattered around zero. We also perform a multiple regression as in Mebust et al. (2011), and derive ECs of  $0.203 \pm 0.042$ ,  $0.290 \pm 0.040$ , and  $0.195 \pm 0.022$  g NO<sub>x</sub> MJ<sup>-1</sup> (as NO) for forest, shrub, and grass fires, respectively. In an absolute sense, these values are lower than those derived in Mebust et al. (2011) by 52 % for shrubs, 34 % for grasses, and 16 % for forests. Much of the decrease is due to generally lower values of tropospheric NO<sub>2</sub> columns in version 2.1 of the NASA OMNO2 standard product relative to version 1.0. Further reduction in the case of shrub fires is due to inclusion of the years 2009–2011 which had generally lower ECs (~26 % below the mean EC for all years).

Title Page

Abstract

Introduction

Conclusions

References

Tables

Figures

◀

▶

◀

▶

Back

Close

Full Screen / Esc

Printer-friendly Version

Interactive Discussion



## Global observations of fire NO<sub>x</sub> emissions

A. K. Mebust and  
R. C. Cohen

[Title Page](#)[Abstract](#)[Introduction](#)[Conclusions](#)[References](#)[Tables](#)[Figures](#)[Back](#)[Close](#)[Full Screen / Esc](#)[Printer-friendly Version](#)[Interactive Discussion](#)

In Mebust et al. (2011) we found that the relative differences between grass, shrub and forest fire ECs derived from OMI and MODIS data reproduced similar relative differences in EFs measured for primarily North American fires in situ. In this analysis, we find that the relative differences in ECs and EFs remain within one standard deviation of one another, though the agreement in the ratio is slightly worse. For example, the ratio of grass to forest fire EFs obtained in Battye and Battye (2002) is  $1.4 \pm 0.8$ ; the ratio of ECs for the same fuels as reported in Mebust et al. (2011) is  $1.2 \pm 0.4$  and in this work is  $1.0 \pm 0.2$ . The ratio between shrub and forest fire ECs in both studies is similarly within one standard deviation of the ratio of shrub and forest fire EFs. As in both Battye and Battye (2002) and Mebust et al. (2011), we find that shrub fires in this region emit more NO<sub>x</sub> per unit energy (or mass) than either grass or forest fires. In both this work and Mebust et al. (2011), we find that forest ECs are higher (relative to grass and shrub fires) than EFs presented in Battye and Battye (2002).

### 5.2.2 Comparison with global EF summaries

There exist several previously published EFs intended for use in global models: an initial comprehensive summary of EFs for many species and fuel types presented by Andreae and Merlet (2001); two updates to that work (Hoelzemann et al., 2004; van der Werf et al., 2010); and a recent summary using a more selective set of observations (Akagi et al., 2011). EFs from each of these references, along with ECs from this work, are shown in Fig. 8 (on different y axes). Values for temperate forest, extratropical forest and chaparral from Akagi et al. (2011) are updated to include observations that were published after the summary (Akagi et al., 2013; Yokelson et al., 2013); these updates are available at <http://bai.acd.ucar.edu/Data/fire/>. We note that EFs in previous studies are derived as the mean of several measurements, and the associated “error” bars shown in Fig. 8 are one standard deviation of the measurements. As we previously discussed, this means they reflect some of the natural variability in individual fire emissions, and are not an estimate of the uncertainty in the mean EF. This uncertainty could be estimated using the number of fires from which the EFs are derived, but this

information is not easily and uniformly accessible and so we do not attempt it. The error bars for our work in Fig. 8 are estimates of the uncertainty in the EC, not the variance in individual measurements, and so they estimate a different quantity than the “error” bars from the other studies and should not be directly compared.

5 The previously published summaries differ substantially from one another, a reflection of the large variability in measured NO<sub>x</sub> EFs for individual fires even within a single global-scale biome, and the relatively small sample size which results in substantial changes to the mean when new measurements are added. We find that our biome-scale ECs fall within a narrower range than all of the previous studies. In a relative  
10 sense, our values compare best with those updated from Akagi et al. (2011), although in forested regions they are generally higher (relative to other biomes). This difference may reflect the improvements in sampling coverage in the full satellite record vs. fire emissions measured in situ. However, it is also plausible that this difference results from a low bias in FRP over forested regions. We estimate the plausible magnitude of  
15 this bias by assuming that the observed difference results entirely from the bias and not from sampling differences; in that case, FRP is biased low by ~ 34 %, ~ 40 %, and ~ 67 % for tropical, temperate, and boreal forest fires, respectively. The difference in bias for boreal forest (vs. tropical and temperate forest) could be due to a higher proportion of burning of ground-level or below-ground burning (e.g. peat) in boreal fires.  
20 While the differences we observe relative to Akagi et al. (2011) are almost certainly varied in source, this nevertheless provides a rough estimate of one plausible bias. We note that this estimate is specific to the accuracy of FRP as it pertains to actively detected fires, not the accuracy of FRP at e.g. 0.5° × 0.5° scale where canopy cover might e.g. completely obscure fires that would otherwise be detected by the MODIS  
25 algorithm.

Detailed information on the EF calculations in Akagi et al. (2011) is available in the Supplement of that paper, and thus we can directly compare regional differences in ECs presented here with the EFs used in Akagi et al. (2011) to examine how consistent our results are beyond broad biome categorizations. Akagi et al. (2011) divide the

**Global observations  
of fire NO<sub>x</sub> emissions**A. K. Mebust and  
R. C. Cohen

Title Page

Abstract

Introduction

Conclusions

References

Tables

Figures



Back

Close

Full Screen / Esc

Printer-friendly Version

Interactive Discussion



## Global observations of fire NO<sub>x</sub> emissions

A. K. Mebust and  
R. C. Cohen

Title Page

Abstract

Introduction

Conclusions

References

Tables

Figures

◀

▶

◀

▶

Back

Close

Full Screen / Esc

Printer-friendly Version

Interactive Discussion



tropical forest NO<sub>x</sub> EF into two EFs: one for tropical evergreen deforestation, and one for tropical dry deforestation that is approximately twice as high. When we calculate ECs separately for forest fires in “monsoonal” and “winter-dry” equatorial regimes, that value is higher (by a factor of 1.89) than the EC calculated for forest fires in the “fully humid” equatorial regime. If these climate classifications provide an adequate proxy for evergreen vs. dry deforestation, this result is consistent with Akagi et al. (2011). We also find that the temperate forest EC from Region J is very slightly below the mean temperate forest EC, and forest fire ECs in the California/Nevada region are even lower than in Region J; this is consistent with results from Akagi et al. (2011) in that measurements of California pine understory EFs made by Burling et al. (2011) are slightly below the mean temperate forest understory EF, and EFs from Oregon wildfires measured by Radke et al. (1991) are below the mean temperate forest EF.

In contrast, in Akagi et al. (2011) EFs reported for tropical forest fires in Mexico (Yokelson et al., 2011) are higher (3–5 g NO<sub>x</sub> as NO kg<sup>-1</sup>) on average than EFs for tropical forest fires in Brazil (1–2 g NO<sub>x</sub> as NO kg<sup>-1</sup>; Ferek et al., 1998; Yokelson et al., 2008), while our analysis suggests that ECs from tropical forests in Mexico and Brazil are similar to each other, with ECs in Mexico slightly lower (see Fig. 3, regions D and E). We also find that ECs for the region that encompasses North and South Carolina in our analysis (region G) are much higher than the mean EC for temperate forests, which is inconsistent with the below-mean (Akagi et al., 2013) or slightly above mean (Burling et al., 2011) EFs in the aggregate EF from Akagi et al. (2011) for this biome.

## 6 Conclusions

We present biome- and ecosystem-resolved NO<sub>x</sub> ECs, based on satellite measurements of tropospheric NO<sub>2</sub> from OMI and of FRP from MODIS, for several different biome and ecosystem categories. These ECs are obtained via a method that was adapted from Mebust et al. (2011) for application to global fires and is also updated to include subsequent years of observations and an improved version of the OMI NO<sub>2</sub>

Global observations  
of fire NO<sub>x</sub> emissionsA. K. Mebust and  
R. C. Cohen

Title Page

Abstract

Introduction

Conclusions

References

Tables

Figures

◀

▶

◀

▶

Back

Close

Full Screen / Esc

Printer-friendly Version

Interactive Discussion



retrieval. We compare our biome-scale ECs with summaries of EFs based on in situ measurements and find that the range of biome-scale ECs observed here is smaller than for EFs in previous works. Our results are for the most part consistent with relative differences in EFs from Akagi et al. (2011) although emissions in forest biomes are relatively higher.

We find that the majority of ecoregion-scale ECs are not statistically significantly different from the corresponding mean biome EC, while biome-scale ECs themselves fall into a narrow range with the smallest EC ( $0.250 \text{ g MJ}^{-1}$ ) fully 70 % of the largest ( $0362 \text{ g MJ}^{-1}$ ) EC. We do, however, observe ecoregion-scale ECs that are both significantly and substantially different from the mean biome EC and/or from the range of biome-scale ECs, demonstrating that there exist regions where mean fire NO<sub>x</sub> emission behavior is very different from the global mean. While mean biome and ecoregion ECs are relatively similar, variability in individual fire ECs remains high. Future efforts should focus on elucidating the particular processes that govern this variability; the observed differences in ECs can hopefully guide these efforts by identifying regions where there are important differences in fire NO<sub>x</sub> emission behavior.

**Supplementary material related to this article is available online at**  
**[http://www.atmos-chem-phys-discuss.net/13/21665/2013/  
acpd-13-21665-2013-supplement.zip](http://www.atmos-chem-phys-discuss.net/13/21665/2013/acpd-13-21665-2013-supplement.zip)**

*Acknowledgements.* This work was supported by the National Aeronautics and Space Administration, grants NNX08AE566 and NNX12AB79G, and by the Department of Energy Office of Science Graduate Fellowship Program (DOE SCGF), made possible in part by the American Recovery and Reinvestment Act of 2009, administered by ORISE-ORAU under contract no. DE-AC05-06OR23100. All opinions expressed in this paper are the authors' and do not necessarily reflect the policies and views of DOE, ORAU, or ORISE. OMI data used in this effort were acquired as part of the activities of NASA's Science Mission Directorate, and are archived and distributed by the Goddard Earth Sciences Data and Information Services Center at <http://disc.sci>.

gsfc.nasa.gov/Aura/data-holdings/OMI/omno2\_v003.shtml. MODIS data are distributed by the Land Processes Distributed Active Archive Center, located at the US Geological Survey Earth Resources Observation and Science Center (<http://lpdaac.usgs.gov>). CFSR and CFSv2 data were obtained through the National Center for Atmospheric Research Computer and Information Systems Laboratory Research Data Archive (<http://rda.ucar.edu/>). Köppen-Geiger climate classification data are available at available at <http://koeppen-geiger.vu-wien.ac.at/present.htm>. We thank S. Akagi for providing additional information regarding EFs published in Akagi et al. (2011).

## References

- 10 Akagi, S. K., Yokelson, R. J., Wiedinmyer, C., Alvarado, M. J., Reid, J. S., Karl, T., Crounse, J. D., and Wennberg, P. O.: Emission factors for open and domestic biomass burning for use in atmospheric models, *Atmos. Chem. Phys.*, 11, 4039–4072, doi:10.5194/acp-11-4039-2011, 2011.
- 15 Akagi, S. K., Yokelson, R. J., Burling, I. R., Meinardi, S., Simpson, I., Blake, D. R., McMeeking, G. R., Sullivan, A., Lee, T., Kreidenweis, S., Urbanski, S., Reardon, J., Griffith, D. W. T., Johnson, T. J., and Weise, D. R.: Measurements of reactive trace gases and variable O<sub>3</sub> formation rates in some South Carolina biomass burning plumes, *Atmos. Chem. Phys.*, 13, 1141–1165, doi:10.5194/acp-13-1141-2013, 2013.
- 20 Andreae, M. O. and Merlet, P.: Emission of trace gases and aerosols from biomass burning, *Global Biogeochem. Cy.*, 15, 955–966, 2001.
- Battye, W. and Battye, R.: Development of emissions inventory methods for wildland fire, U.S. Environmental Protection Agency, Research Triangle Park, NC, Contract 68-D-98-046, 2002.
- Boersma, K. F., Bucsela, E., Brinksma, E., and Gleason, J. F.: NO<sub>2</sub>, in: OMI Algorithm Theoretical Basis Document, Volume IV: OMI Trace Gas Algorithms, 2 ed., edited by: Chance, K., 25 Smithsonian Astrophysical Observatory, Cambridge, MA, 13–36, 2002.
- Boersma, K. F., Eskes, H. J., Dirksen, R. J., van der A, R. J., Veefkind, J. P., Stammes, P., Huijnen, V., Kleipool, Q. L., Sneep, M., Claas, J., Leitão, J., Richter, A., Zhou, Y., and Brunner, D.: An improved tropospheric NO<sub>2</sub> column retrieval algorithm for the Ozone Monitoring Instrument, *Atmos. Meas. Tech.*, 4, 1905–1928, doi:10.5194/amt-4-1905-2011, 2011.

## Global observations of fire NO<sub>x</sub> emissions

A. K. Mebust and  
R. C. Cohen

Title Page

Abstract

Introduction

Conclusions

References

Tables

Figures

◀

▶

◀

▶

Back

Close

Full Screen / Esc

Printer-friendly Version

Interactive Discussion



Global observations  
of fire NO<sub>x</sub> emissionsA. K. Mebust and  
R. C. Cohen

Title Page

Abstract

Introduction

Conclusions

References

Tables

Figures

◀

▶

◀

▶

Back

Close

Full Screen / Esc

Printer-friendly Version

Interactive Discussion

- Boschetti, L. and Roy, D. P.: Strategies for the fusion of satellite fire radiative power with burned area data for fire radiative energy derivation, *J. Geophys. Res. Atmos.*, 114, D20302, doi:10.1029/2008JD011645, 2009.
- 5 Bowman, D. M. J. S., Balch, J. K., Artaxo, P., Bond, W. J., Carlson, J. M., Cochrane, M. A., D'Antonio, C. M., DeFries, R. S., Doyle, J. C., Harrison, S. P., Johnston, F. H., Keeley, J. E., Krawchuk, M. A., Kull, C. A., Marston, J. B., Moritz, M. A., Prentice, I. C., Roos, C. I., Scott, A. C., Swetnam, T. W., van der Werf, G. R., and Pyne, S. J.: Fire in the Earth System, *Science*, 324, 481–484, 2009.
- 10 Bucsela, E. J., Krotkov, N. A., Celarier, E. A., Lamsal, L. N., Swartz, W. H., Bhartia, P. K., Boersma, K. F., Veefkind, J. P., Gleason, J. F., and Pickering, K. E.: A new stratospheric and tropospheric NO<sub>2</sub> retrieval algorithm for nadir-viewing satellite instruments: applications to OMI, *Atmos. Meas. Tech. Discuss.*, 6, 1361–1407, doi:10.5194/amtd-6-1361-2013, 2013.
- 15 Burling, I. R., Yokelson, R. J., Akagi, S. K., Urbanski, S. P., Wold, C. E., Griffith, D. W. T., Johnson, T. J., Reardon, J., and Weise, D. R.: Airborne and ground-based measurements of the trace gases and particles emitted by prescribed fires in the United States, *Atmos. Chem. Phys.*, 11, 12197–12216, doi:10.5194/acp-11-12197-2011, 2011.
- Ferek, R. J., Reid, J. S., Hobbs, P. V., Blake, D. R., and Liousse, C.: Emission factors of hydrocarbons, halocarbons, trace gases and particles from biomass burning in Brazil, *J. Geophys. Res. Atmos.*, 103, 32107–32118, 1998.
- 20 Fiore, A. M., Naik, V., Spracklen, D. V., Steiner, A., Unger, N., Prather, M., Bergmann, D., Cameron-Smith, P. J., Cionni, I., Collins, W. J., Dalsoren, S., Eyring, V., Folberth, G. A., Ginoux, P., Horowitz, L. W., Josse, B., Lamarque, J. F., MacKenzie, I. A., Nagashima, T., O'Connor, F. M., Righi, M., Rumbold, S. T., Shindell, D. T., Skeie, R. B., Sudo, K., Szopa, S., Takemura, T., and Zeng, G.: Global air quality and climate, *Chem. Soc. Rev.*, 41, 6663–6683, 2012.
- 25 Freeborn, P. H., Wooster, M. J., Hao, W. M., Ryan, C. A., Nordgren, B. L., Baker, S. P., and Ichoku, C.: Relationships between energy release, fuel mass loss, and trace gas and aerosol emissions during laboratory biomass fires, *J. Geophys. Res.*, 113, D01301, doi:10.1029/2007JD008679, 2008.
- 30 Freeborn, P. H., Wooster, M. J., and Roberts, G.: Addressing the spatiotemporal sampling design of MODIS to provide estimates of the fire radiative energy emitted from Africa, *Remote Sens. Environ.*, 115, 475–489, 2011.

Global observations  
of fire NO<sub>x</sub> emissionsA. K. Mebust and  
R. C. Cohen

Title Page

Abstract

Introduction

Conclusions

References

Tables

Figures

◀

▶

◀

▶

Back

Close

Full Screen / Esc

Printer-friendly Version

Interactive Discussion

- Friedl, M. A., Sulla-Menashe, D., Tan, B., Schneider, A., Ramankutty, N., Sibley, A., and Huang, X. M.: MODIS Collection 5 global land cover: Algorithm refinements and characterization of new datasets, *Remote Sens. Environ.*, 114, 168–182, 2010.
- 5 Giglio, L., Descloitres, J., Justice, C. O., and Kaufman, Y. J.: An enhanced contextual fire detection algorithm for MODIS, *Remote Sens. Environ.*, 87, 273–282, 2003.
- Granier, C., Bessagnet, B., Bond, T., D'Angiola, A., van der Gon, H. D., Frost, G. J., Heil, A., Kaiser, J. W., Kinne, S., Klimont, Z., Kloster, S., Lamarque, J. F., Liousse, C., Masui, T., Meleux, F., Mieville, A., Ohara, T., Raut, J. C., Riahi, K., Schultz, M. G., Smith, S. J., Thompson, A., van Aardenne, J., van der Werf, G. R., and van Vuuren, D. P.: Evolution of anthropogenic and biomass burning emissions of air pollutants at global and regional scales during the 1980–2010 period, *Climatic Change*, 109, 163–190, 2011.
- 10 Hoelzemann, J. J., Schultz, M. G., Brasseur, G. P., Granier, C., and Simon, M.: Global Wildland Fire Emission Model (GWEM): Evaluating the use of global area burnt satellite data, *J. Geophys. Res.*, 109, D14S04, doi:10.1029/2003JD003666, 2004.
- 15 Ichoku, C. and Kaufman, Y. J.: A method to derive smoke emission rates from MODIS fire radiative energy measurements, *IEEE Trans. Geosci. Remote Sens.*, 43, 2636–2649, 2005.
- Jacob, D. J., Crawford, J. H., Maring, H., Clarke, A. D., Dibb, J. E., Emmons, L. K., Ferrare, R. A., Hostetler, C. A., Russell, P. B., Singh, H. B., Thompson, A. M., Shaw, G. E., McCauley, E., Pederson, J. R., and Fisher, J. A.: The Arctic Research of the Composition of the Troposphere from Aircraft and Satellites (ARCTAS) mission: design, execution, and first results, *Atmos. Chem. Phys.*, 10, 5191–5212, doi:10.5194/acp-10-5191-2010, 2010.
- 20 Jaffe, D. A. and Wigder, N. L.: Ozone production from wildfires: A critical review, *Atmos. Environ.*, 51, 1–10, 2012.
- Jordan, N. S., Ichoku, C., and Hoff, R. M.: Estimating smoke emissions over the US Southern Great Plains using MODIS fire radiative power and aerosol observations, *Atmos. Environ.*, 42, 2007–2022, 2008.
- 25 Justice, C. O., Giglio, L., Korontzi, S., Owens, J., Morissette, J. T., Roy, D., Descloitres, J., Al-leaume, S., Petitcolin, F., and Kaufman, Y.: The MODIS fire products, *Remote Sens. Environ.*, 83, 244–262, 2002.
- 30 Kaufman, Y. J., Justice, C. O., Flynn, L. P., Kendall, J. D., Prins, E. M., Giglio, L., Ward, D. E., Menzel, W. P., and Setzer, A. W.: Potential global fire monitoring from EOS-MODIS, *J. Geophys. Res.*, 103, 32215–32238, 1998.

Global observations  
of fire NO<sub>x</sub> emissionsA. K. Mebust and  
R. C. Cohen

Title Page

Abstract

Introduction

Conclusions

References

Tables

Figures

◀

▶

◀

▶

Back

Close

Full Screen / Esc

Printer-friendly Version

Interactive Discussion

- Korontzi, S., Ward, D. E., Susott, R. A., Yokelson, R. J., Justice, C. O., Hobbs, P. V., Smithwick, E. A. H., and Hao, W. M.: Seasonal variation and ecosystem dependence of emission factors for selected trace gases and PM<sub>2.5</sub> for southern African savanna fires, *J. Geophys. Res.*, 108, 4758, doi:10.1029/2003JD003730, 2003.
- 5 Kottek, M., Grieser, J., Beck, C., Rudolf, B., and Rubel, F.: World map of the Koppen-Geiger climate classification updated, *Meteorol. Z.*, 15, 259–263, 2006.
- Lacaux, J. P., Delmas, R., Jambert, C., and Kuhlbusch, T. A. J.: NO<sub>x</sub> emissions from African savanna fires, *J. Geophys. Res.*, 101, 23585–23595, 1996.
- Leitão, J., Richter, A., Vrekoussis, M., Kokhanovsky, A., Zhang, Q. J., Beekmann, M., and Burrows, J. P.: On the improvement of NO<sub>2</sub> satellite retrievals – aerosol impact on the air mass factors, *Atmos. Meas. Tech.*, 3, 475–493, doi:10.5194/amt-3-475-2010, 2010.
- 10 Mebust, A. K. and Cohen, R. C.: Observations of a seasonal cycle in NO<sub>x</sub> emissions from fires in African woody savannas, *Geophys. Res. Lett.*, 40, 1451–1455, 2013.
- Mebust, A. K., Russell, A. R., Hudman, R. C., Valin, L. C., and Cohen, R. C.: Characterization of wildfire NO<sub>x</sub> emissions using MODIS fire radiative power and OMI tropospheric NO<sub>2</sub> columns, *Atmos. Chem. Phys.*, 11, 5839–5851, doi:10.5194/acp-11-5839-2011, 2011.
- Monfreda, C., Ramankutty, N., and Foley, J. A.: Farming the planet: 2. Geographic distribution of crop areas, yields, physiological types, and net primary production in the year 2000, *Global Biogeochem. Cy.*, 22, GB1022, doi:10.1029/2007GB002947, 2008.
- 20 Radke, L. F., Hegg, D. A., Hobbs, P. V., Nance, J. D., Lyons, J. H., Laursen, K. K., Weiss, R. E., Riggan, P. J., and Ward, D. E.: Particulate and trace gas emissions from large biomass fires in North America, in: *Global biomass burning – Atmospheric, climatic, and biospheric implications*, MIT Press, Cambridge, MA, 209–224, 1991.
- Russell, A. R., Perring, A. E., Valin, L. C., Bucsela, E. J., Browne, E. C., Wooldridge, P. J., and Cohen, R. C.: A high spatial resolution retrieval of NO<sub>2</sub> column densities from OMI: method and evaluation, *Atmos. Chem. Phys.*, 11, 8543–8554, doi:10.5194/acp-11-8543-2011, 2011.
- 25 Saha, S., Moorthi, S., Pan, H. L., Wu, X. R., Wang, J. D., Nadiga, S., Tripp, P., Kistler, R., Woollen, J., Behringer, D., Liu, H. X., Stokes, D., Grumbine, R., Gayno, G., Wang, J., Hou, Y. T., Chuang, H. Y., Juang, H. M. H., Sela, J., Iredell, M., Treadon, R., Kleist, D., Van Delst, P., Keyser, D., Derber, J., Ek, M., Meng, J., Wei, H. L., Yang, R. Q., Lord, S., Van den Dool, H., Kumar, A., Wang, W. Q., Long, C., Chelliah, M., Xue, Y., Huang, B. Y., Schemm, J. K., Ebisuzaki, W., Lin, R., Xie, P. P., Chen, M. Y., Zhou, S. T., Higgins, W., Zou, C. Z., Liu, Q. H.,
- 30

Global observations  
of fire NO<sub>x</sub> emissionsA. K. Mebust and  
R. C. Cohen

Title Page

Abstract

Introduction

Conclusions

References

Tables

Figures

◀

▶

◀

▶

Back

Close

Full Screen / Esc

Printer-friendly Version

Interactive Discussion



Chen, Y., Han, Y., Cucurull, L., Reynolds, R. W., Rutledge, G., and Goldberg, M.: The NCEP Climate Forecast System Reanalysis, *B. Am. Meteorol. Soc.*, 91, 1015–1057, 2010.

Saha, S., Moorthi, S., Wu, X., Wang, J., Nadiga, S., Tripp, P., Behringer, D., Hou, Y.-T., Chuang, H.-y., Iredell, M., Ek, M., Meng, J., Yang, R., Mendez, M. P., Dool, H. v. d., Zhang, Q., Wang, W., Chen, M., and Becker, E.: The NCEP Climate Forecast System Version 2, *J. Climate*, submitted, 2013.

Simpson, I. J., Akagi, S. K., Barletta, B., Blake, N. J., Choi, Y., Diskin, G. S., Fried, A., Fuelberg, H. E., Meinardi, S., Rowland, F. S., Vay, S. A., Weinheimer, A. J., Wennberg, P. O., Wiebring, P., Wisthaler, A., Yang, M., Yokelson, R. J., and Blake, D. R.: Boreal forest fire emissions in fresh Canadian smoke plumes: C1–C10 volatile organic compounds (VOCs), CO<sub>2</sub>, CO, NO<sub>2</sub>, NO, HCN and CH<sub>3</sub>CN, *Atmos. Chem. Phys.*, 11, 6445–6463, doi:10.5194/acp-11-6445-2011, 2011.

van der Werf, G. R., Randerson, J. T., Giglio, L., Collatz, G. J., Mu, M., Kasibhatla, P. S., Morton, D. C., DeFries, R. S., Jin, Y., and van Leeuwen, T. T.: Global fire emissions and the contribution of deforestation, savanna, forest, agricultural, and peat fires (1997–2009), *Atmos. Chem. Phys.*, 10, 11707–11735, doi:10.5194/acp-10-11707-2010, 2010.

van Leeuwen, T. T. and van der Werf, G. R.: Spatial and temporal variability in the ratio of trace gases emitted from biomass burning, *Atmos. Chem. Phys.*, 11, 3611–3629, doi:10.5194/acp-11-3611-2011, 2011.

van Leeuwen, T. T., Peters, W., Krol, M. C., and van der Werf, G. R.: Dynamic biomass burning emission factors and their impact on atmospheric CO mixing ratios, *J. Geophys. Res. Atmos.*, 118, 6797–6815, doi:10.1002/jgrd.50478, 2013.

Vermote, E., Ellicott, E., Dubovik, O., Lapyonok, T., Chin, M., Giglio, L., and Roberts, G. J.: An approach to estimate global biomass burning emissions of organic and black carbon from MODIS fire radiative power, *J. Geophys. Res.*, 114, D18205, doi:10.1029/2008JD011188, 2009.

Wiedinmyer, C., Quayle, B., Geron, C., Belote, A., McKenzie, D., Zhang, X. Y., O'Neill, S., and Wynne, K. K.: Estimating emissions from fires in North America for air quality modeling, *Atmos. Environ.*, 40, 3419–3432, 2006.

Wooster, M. J.: Small-scale experimental testing of fire radiative energy for quantifying mass combusted in natural vegetation fires, *Geophys. Res. Lett.*, 29, 2027, doi:10.1029/2002GL015487, 2002.

Global observations  
of fire NO<sub>x</sub> emissionsA. K. Mebust and  
R. C. Cohen

Title Page

Abstract

Introduction

Conclusions

References

Tables

Figures

◀

▶

◀

▶

Back

Close

Full Screen / Esc

Printer-friendly Version

Interactive Discussion



Wooster, M. J., Zhukov, B., and Oertel, D.: Fire radiative energy for quantitative study of biomass burning: derivation from the BIRD experimental satellite and comparison to MODIS fire products, *Remote Sens. Environ.*, 86, 83–107, 2003.

5 Wooster, M. J., Roberts, G., Perry, G. L. W., and Kaufman, Y. J.: Retrieval of biomass combustion rates and totals from fire radiative power observations: FRP derivation and calibration relationships between biomass consumption and fire radiative energy release, *J. Geophys. Res.*, 110, D24311, doi:10.1029/2005JD006318, 2005.

10 Yokelson, R. J., Christian, T. J., Karl, T. G., and Guenther, A.: The tropical forest and fire emissions experiment: laboratory fire measurements and synthesis of campaign data, *Atmos. Chem. Phys.*, 8, 3509–3527, doi:10.5194/acp-8-3509-2008, 2008.

Yokelson, R. J., Burling, I. R., Urbanski, S. P., Atlas, E. L., Adachi, K., Buseck, P. R., Wiedinmyer, C., Akagi, S. K., Toohey, D. W., and Wold, C. E.: Trace gas and particle emissions from open biomass burning in Mexico, *Atmos. Chem. Phys.*, 11, 6787–6808, doi:10.5194/acp-11-6787-2011, 2011.

15 Yokelson, R. J., Burling, I. R., Gilman, J. B., Warneke, C., Stockwell, C. E., de Gouw, J., Akagi, S. K., Urbanski, S. P., Veres, P., Roberts, J. M., Kuster, W. C., Reardon, J., Griffith, D. W. T., Johnson, T. J., Hosseini, S., Miller, J. W., Cocker III, D. R., Jung, H., and Weise, D. R.: Coupling field and laboratory measurements to estimate the emission factors of identified and unidentified trace gases for prescribed fires, *Atmos. Chem. Phys.*, 13, 89–116, doi:10.5194/acp-13-89-2013, 2013.

20

Global observations  
of fire NO<sub>x</sub> emissionsA. K. Mebust and  
R. C. Cohen

Title Page

Abstract

Introduction

Conclusions

References

Tables

Figures

◀

▶

◀

▶

Back

Close

Full Screen / Esc

Printer-friendly Version

Interactive Discussion

**Table 1.** Classification of IGBP classes to broad biome categories.

IGBP class	Biome category
Water	Not assigned
Evergreen needleleaf forest	Forest
Evergreen broadleaf forest	Forest
Deciduous needleleaf forest	Forest
Deciduous broadleaf forest	Forest
Mixed forest	Forest
Closed shrublands	Shrub
Open shrublands	Shrub
Woody savannas	Grass
Savannas	Grass
Grasslands	Grass
Permanent wetlands	Not assigned
Croplands	Agricultural
Urban and built-up	Not assigned
Cropland/natural vegetation mosaic	Not assigned
Snow and ice	Not assigned
Barren/sparsely vegetated	Not assigned

Global observations  
of fire NO<sub>x</sub> emissionsA. K. Mebust and  
R. C. Cohen**Table 2.** Summary of calculated emission coefficients and emission factors for NO<sub>x</sub> as NO.

Fuel type	NO <sub>x</sub> EC (g MJ <sup>-1</sup> ) <sup>a</sup>	NO <sub>x</sub> EF (g kg <sup>-1</sup> ) <sup>a,b</sup>	<i>N</i>	<i>R</i> <sup>2</sup>
Tropical forests	0.356 ± 0.044	0.87 ± 0.11	6266	0.307
Temperate forests	0.298 ± 0.019	0.727 ± 0.047	3417	0.293
Boreal forests	0.250 ± 0.033	0.609 ± 0.079	1633	0.308
Extratropical forests <sup>c</sup>	0.275 ± 0.020	0.670 ± 0.049	5050	0.298
Grasslands	0.362 ± 0.015	0.883 ± 0.037	73789	0.290
Shrublands	0.275 ± 0.030	0.671 ± 0.075	4764	0.439
Agriculture	0.266 ± 0.024	0.650 ± 0.061	4732	0.068

<sup>a</sup> Assumes 75 % of NO<sub>x</sub> is present as NO<sub>2</sub>. <sup>b</sup> Calculated using a value of 0.41 kg MJ<sup>-1</sup> (Vermote et al., 2009). <sup>c</sup> Extratropical forests include both boreal and temperate forests.

Title Page

Abstract

Introduction

Conclusions

References

Tables

Figures

◀

▶

◀

▶

Back

Close

Full Screen / Esc

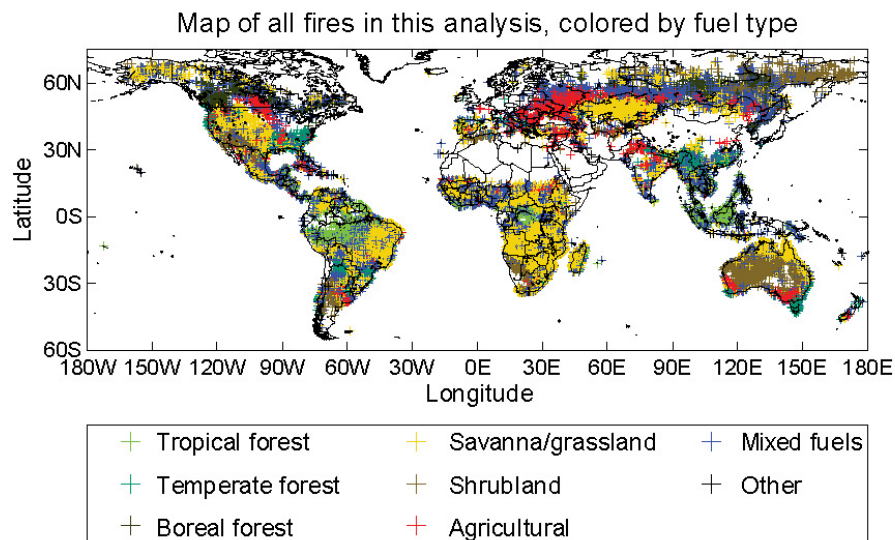
Printer-friendly Version

Interactive Discussion



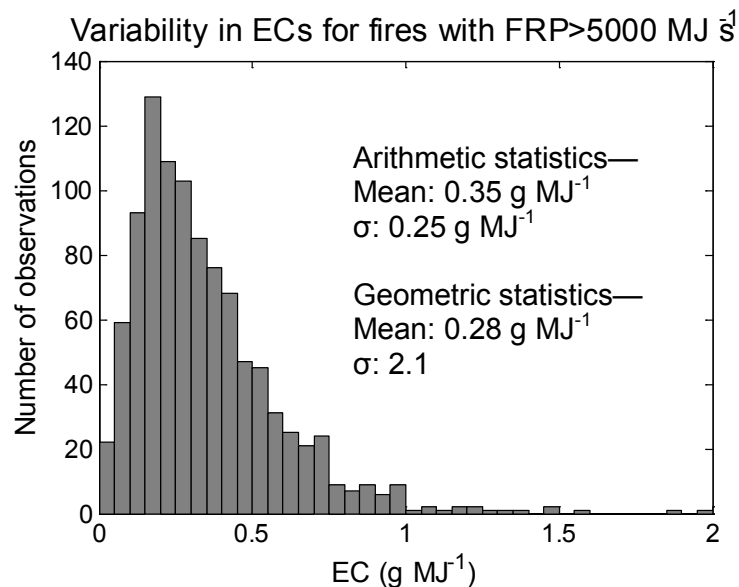
## Global observations of fire NO<sub>x</sub> emissions

A. K. Mebust and  
R. C. Cohen



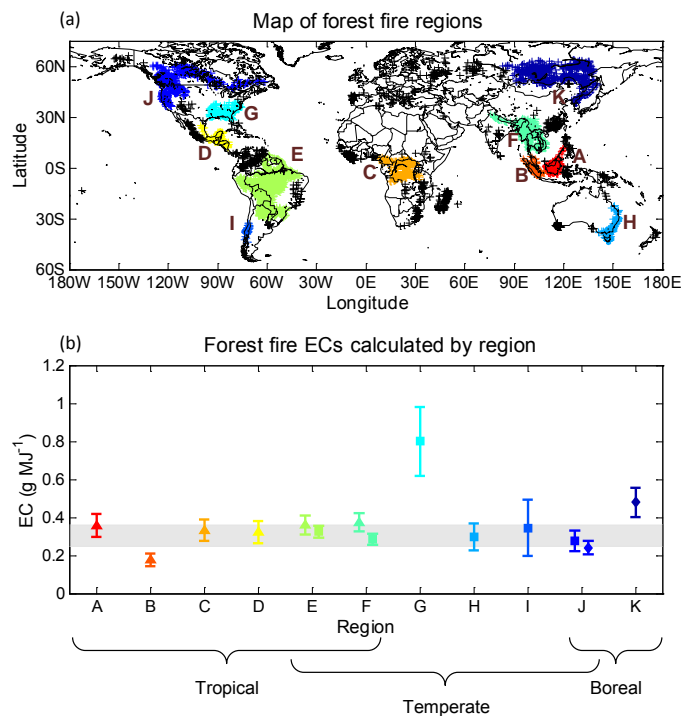
**Fig. 1.** Map of fires used in this analysis. Color indicates fuel type as determined using land cover and climatology. Fires were identified as having a particular fuel if greater than 75 % of measured FRP for that fire came from fire pixels of a single fuel type; fires not meeting this criterion are designated “mixed fuels”.

[Title Page](#)
[Abstract](#)
[Introduction](#)
[Conclusions](#)
[References](#)
[Tables](#)
[Figures](#)
[◀](#)
[▶](#)
[◀](#)
[▶](#)
[Back](#)
[Close](#)
[Full Screen / Esc](#)
[Printer-friendly Version](#)
[Interactive Discussion](#)

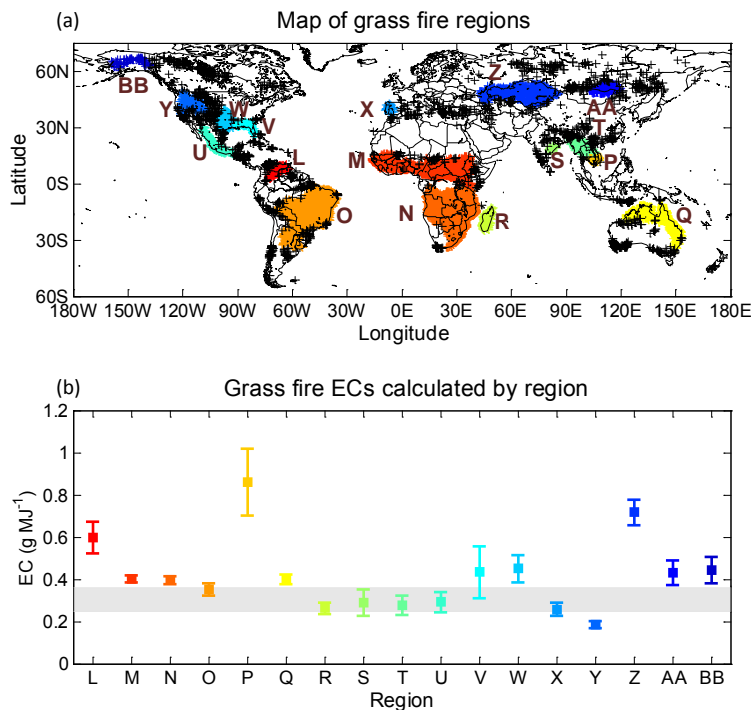

Global observations  
of fire  $\text{NO}_x$  emissionsA. K. Mebust and  
R. C. Cohen

**Fig. 2.** Histogram of ECs measured for fires with FRP above  $5000 \text{ MJ s}^{-1}$ . ECs were calculated by dividing the MER by FRP for individual fires.

[Title Page](#)[Abstract](#)[Introduction](#)[Conclusions](#)[References](#)[Tables](#)[Figures](#)[◀](#)[▶](#)[◀](#)[▶](#)[Back](#)[Close](#)[Full Screen / Esc](#)[Printer-friendly Version](#)[Interactive Discussion](#)

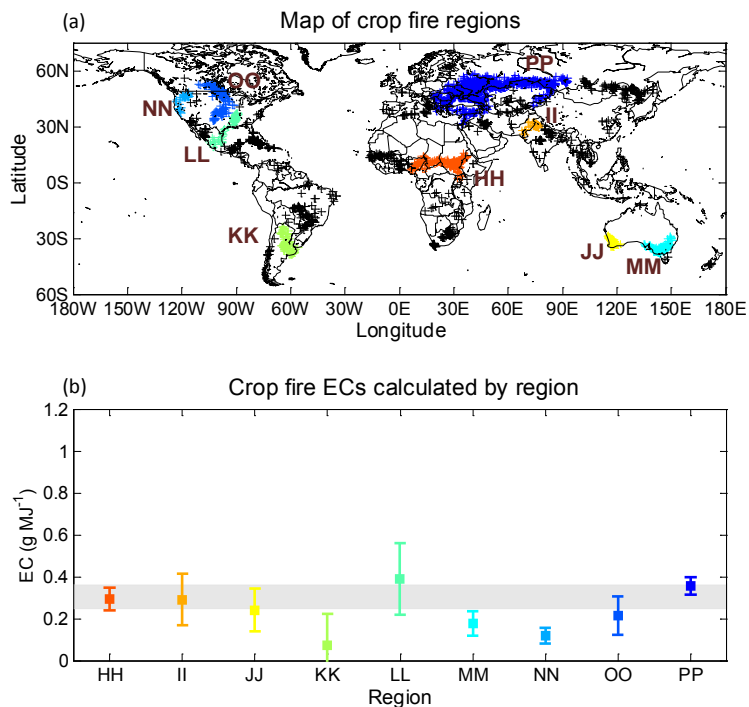
Global observations of fire NO<sub>x</sub> emissionsA. K. Mebust and  
R. C. Cohen

**Fig. 3.** A map of forest fire regions determined by a clustering analysis (a) and ECs calculated individually for each region (b). In (a), black markers identify forest fires belonging to clusters with less than 100 observations. In (b), marker shapes are used to identify biomes for each EC, determined via climate classifications: triangles indicate tropical, squares indicate temperate, and diamonds indicate boreal forests. In regions where there is adequate sampling of more than one biome type, ECs are calculated for both biomes (e.g. Region E). The range of mean biome ECs (as presented in Table 2) is indicated in grey.

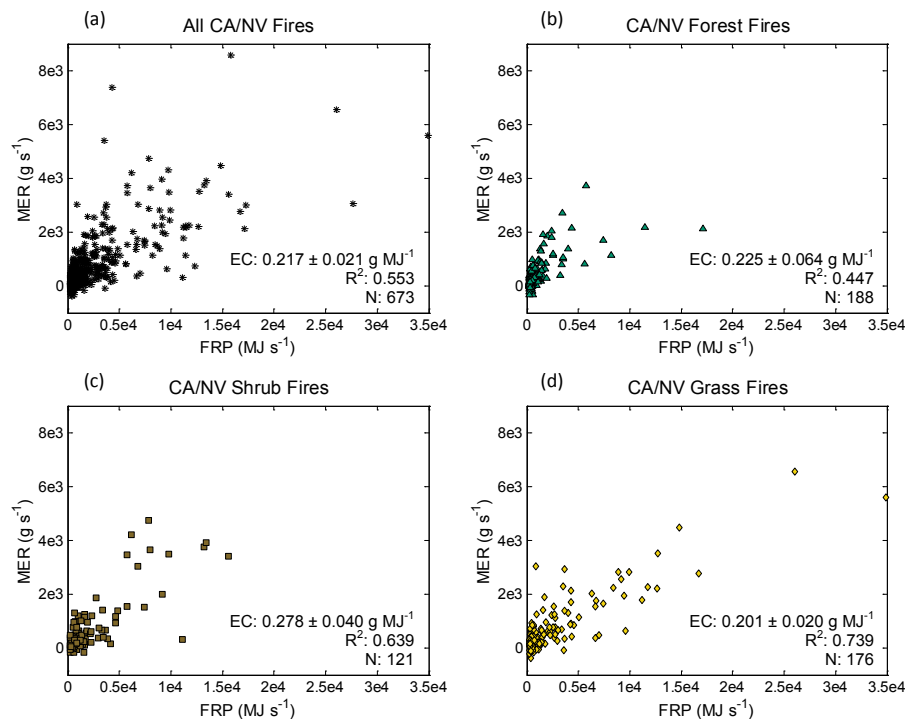
Global observations  
of fire NO<sub>x</sub> emissionsA. K. Mebust and  
R. C. Cohen

**Fig. 4.** A map of grass fire regions determined by a clustering analysis **(a)** and ECs calculated individually for each region **(b)**. In **(a)**, black markers identify grass fires belonging to clusters with less than 100 observations. In **(b)**, the range of mean biome ECs (as presented in Table 2) is indicated in grey.

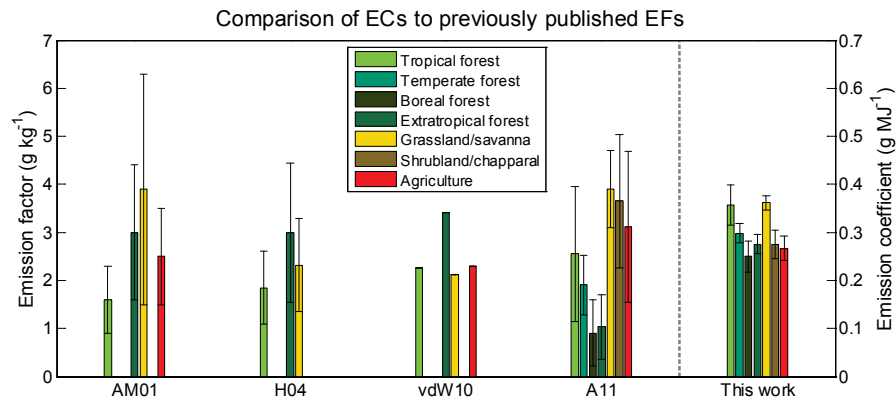


Global observations  
of fire  $\text{NO}_x$  emissionsA. K. Mebust and  
R. C. Cohen

**Fig. 6.** A map of agricultural fire regions determined by a clustering analysis **(a)** and ECs calculated individually for each region **(b)**. In **(a)**, black markers identify agricultural fires belonging to clusters with less than 100 observations. In **(b)**, the range of mean biome ECs (as presented in Table 2) is indicated in grey.

Global observations  
of fire NO<sub>x</sub> emissionsA. K. Mebust and  
R. C. Cohen

**Fig. 7.** Regressions of fire radiative power (FRP) vs. mass emission rate (MER) for **(a)** all fires, **(b)** forest fires, **(c)** shrub fires and **(d)** grass fires in the California/Nevada region (126–113° W, 31–44° N). Listed on each plot are the calculated EC (i.e. the slope of the best fit line),  $R^2$ , and number of points.

Global observations  
of fire NO<sub>x</sub> emissionsA. K. Mebust and  
R. C. Cohen

**Fig. 8.** Bar graph showing the different EFs (left y axis) in previous work and ECs (right y axis) presented here at the global biome scale. EFs from previous studies (from left to right) are: Andreae and Merlet (2001), Hoelzemann et al. (2004), van der Werf et al. (2010), Akagi et al. (2011). In previous work, error bars indicate one standard deviation of the mean; in the case of van der Werf et al. (2010), no standard deviation was reported. Error bars for this work indicate the standard error of the fit.